



1 Article

9

21

22

23

24

25

26

27

28

29

30

31

32

33

34

35

36

37

38

39

40

41

42

43

2 An electrokinetically-driven microchip for rapid

3 extraction and detection of nanovesicles

- 4 Leilei Shi 1, Leyla Esfandiari 1,2,*
- Department of Electrical Engineering and Computer Science, College of Engineering and Applied Sciences,
 University of Cincinnati, Ohio, 45221, United States
- Department of Biomedical Engineering, College of Engineering and Applied Sciences, University of Cincinnati, Ohio, 45221, United States
 - * Correspondence: esfandla@ucmail.uc.edu
- Received: date; Accepted: date; Published: date
- 11 Abstract: Electrical Impedance Spectroscopy (EIS) has been widely used as a label-free and rapid 12 characterization method for analysis of cells in clinical research. However, the related work on sub-13 micron bioparticles has not yet been reported. In this study, we developed a new Lab-on-a-Chip 14 (LOC) device to rapidly entrap a cluster of sub-micron particles, including polystyrene beads, 15 liposomes and small extracellular vesicles (exosomes), utilizing an insulator-based dielectrophoresis 16 (iDEP) scheme followed by measuring their impedance utilizing an integrated electrical impedance 17 sensor. This technique provides a label-free, fast, and non-invasive tool for detection of 18 bionanoparticles based on their unique dielectric properties. In future, this device could potentially 19 be applied for characterization of pathogenic exosomes and viruses with similar size, and thus, be 20 evolved as a powerful tool for early disease diagnosis and prognosis.
 - **Keywords:** Nanovesicle; Biological Nanoparticles; Exosome; Impedance; Dielectrophoresis; Biosensing; Microfluidics; Lab-on-a-chip

1. Introduction

Electrical Impedance Spectroscopy (EIS) has been desirable for characterization of various biological entities, since it can be used as a label-free method with minimal sample preparation procedure.[1-8] This technique has been used to differentiate various cell types and to identify the abnormal or tumor cells. [9,10] One popular design for EIS is the single cell impedance cytometry, in which a pair of facing or coplanar electrodes are embedded in a microfluidic channel. [2,3,5,11-15] The electrodes are energized with a voltage at one or more discrete frequencies, generating an electric field within the channel. As cells pass through the microfluidic channel one at a time, the fluctuation of the electric current is detected, and thus, provides the impedance of a single cell. Another strategy is based on the static state impedance measurement approach, in which a single cell is manipulated to be placed at the center of the electrodes, and thus, the electric field in the detection volume is altered due to the presence of the cell.[4,10,16] However, the related work on sub-micron particles and small extracellular vesicles (exosomes) with diameters of 40-150 nm has not yet been reported. The main challenge for adapting this system for analysis of a single vesicle is that the scale of the channel and/or electrodes must be miniaturized to the corresponding size scale of the target vesicle in order to achieve a reliable sensitivity.[4] Although the device with miniaturized channel and electrodes could be fabricated, it is very challenging to pass a single vesicle one at a time through the channel or manipulate it to the designated position. In addition, a high applied pressure would be needed to overcome the high resistance of the submicron channel to omit the channel's blockage by the vesicles.

We have previously demonstrated that a new insulator-based dielectrophoretic (iDEP) device made of an array of micropipettes can be utilized for rapid entrapment of nanovesicles based on their unique dielectric properties at pipettes' pores; due to the balance of three electrokinteic forces including dielectrophoretic (DEP), electrophoretic (EP), and electroosmotic (EOF) forces.[17,18] In this paper, we have fabricated a microchip to rapidly entrap a cluster of vesicles utilizing an iDEP scheme by applying a direct current (DC) followed by simultaneously measuring their impedance by an embedded microelectrodes and applying an alternative current (AC) at a wide frequency spectrum. In addition, electrolyte solutions with different ionic strengths with and without suspended particles have been utilized to study the capability of the device to differentiate between nanoparticles with different dielectric properties. The microchip was able to differentiate between various sub-micron particles of similar size, including polystyrene beads, liposomes and exosomes and thus, it has the potential to further be evolved as a characterization tool for differentiation of circulating nanovesicles for diagnosis purposes

2. Materials and Methods

2.1. Materials

All chemicals were purchased from Sigma-Aldrich (St. Louis, MO, USA) unless otherwise noted. 100 nm carboxylic acid polystyrene (COOH-PS) beads were obtained from Phosphorex Inc. (Hopkinton, MA, USA). N-(7-nitrobenz-2-oxa-1,3-diazol-4-yl)-1,2-dihexadecanoyl-sn-glycero-3-phosphoethanolamine (NBD-DHPE) fluorescently labeled 100 nm liposomes were purchased from FormuMax Scientific Inc. (Sunnyvale, CA, USA). Telomerase reverse transcriptase (hTERT) Mesenchymal Stem Cell Exosomes with the average diameter of 146 nm were purchased from ATCC (Manassas, VA, USA). Silicone elastomer base and curing agent were purchased from Dow Corning (Elizabethtown, KY). Gold etchant (Type TFA) and chromium etchant (1020AC) were obtained from Transene Company Inc. (Danvers, MA, USA). Photoresist AZ5214E and developer AZ917 MIF were purchased from Integrated Micro Materials (Argyle, TX, USA). SU-8 2050, SU-8 developer and OmniCoat were obtained from Microchem Corp. (Westborough, MA, USA). Polyimide PI2610 and adhesion promoter MV652 were obtained from Hitachi DuPont MicroSystems LLC. (Parlin, NJ, USA). Heat seal connectors were obtained from Elform Inc. (Reno, NV, USA). The printed circuit board (PCB) was fabricated by PCB Universe (Vancouver, WA, USA). Glass slides were purchased from Ted Pella Inc. (Redding, CA, USA).

2.2. Preparation of sub-micron particles

Electrolyte solutions containing different potassium chloride (KCl) concentrations (1 mM, 10 mM, 500 mM) were prepared at pH 7.0. The conductivity of KCl solutions were measured utilizing a conductivity meter (Oakton Cond 6+) as: 0.3 S/m for 10 mM KCl, 1.4 S/m for 100 mM KCl, and 5.9 S/m for 500 mM KCl.

100 nm COOH-PS beads were re-suspended into 10 mM KCl to the final concentration of 1.8×10⁸ /mL and 2.3×10¹² /mL. 100 nm liposomes were re-suspended into 10 mM KCl at a final concentration of 1.9×10¹¹ /mL. 146 nm hTERT Mesenchymal Stem Cell Exosomes were distributed in 10 mM KCl with the concentration of 6.1×10⁹ /mL. The zeta potential of COOH-PS beads, liposomes, and exosomes dispersed in 10 mM KCl at 25°C were measured at least 3 times using the Zetasizer-NanoBrook Omni (Brookhaven Instruments, NY, USA).

2.3. Device layout and fabrication

The LOC device was designed with AutoCAD 2018. A cross-sectional view of the LOC device was shown in Fig. 1, which contained seven layers as follow: the glass substrate, the first polyimide (PI) layer to improve the adhesion strength of the substrate, the sensing electrodes, second PI layer to avoid short circuit of different electrode layers, the trapping electrodes, the SU-8 obstacles, and the PDMS chambers.

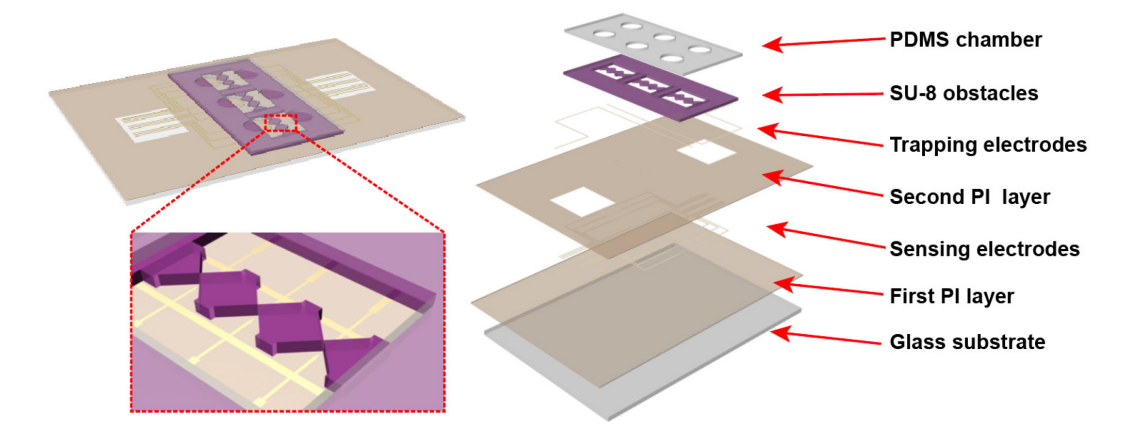


Figure 1. Schematic of the LOC device including the iDEP module for particle trapping (PDMS chamber, SU-8 obstacles, and Trapping electrodes) and the impedance sensing module (Sensing electrodes).

The first PI layer was deposited to increase the adhesion between gold and the glass substrate. Prior to the deposition of PI, adhesion promoter VM652 was spin-coated at 2000 rpm for 30 seconds. PI2610 was then spread at 500 rpm for 5 seconds followed by 5000 rpm for 30 seconds to form a 1 μ m thin film (Fig. 2a). To fabricate the sensing electrodes, a layer of metal (10 nm Cr and 200 nm Au) was deposited on the PI-coated substrate using the E-beam evaporator (Fig. 2b). The deposited metal was patterned using the photolithography technique with AZ5214E as the positive photoresist and MIF 917 as the developer. A pair of digital sensing electrode array was then created by etching the redundant Au and Cr on the first metal layer. Afterwards, the photoresist residual was removed by acetone (Fig. 2c). Prior to the deposition of trapping electrodes, adhesion promoter VM652 and PI2610 were spincoated to insulate the sensing electrodes (Fig. 2d). 10 nm Cr and 200 nm Au were then deposited (Fig. 2e) and patterned (Fig. 2f). EVG620 mask aligner was used to align the trapping and the sensing electrodes. The width and the length of each trapping electrode was designed to be 0.25 mm and 26 mm, and the distance between the trapping electrodes was 2 mm. In order to connect the sensing electrodes with the digital impedance analyzer (HF2LI, Zurich Instrument), the PI film that covered the corresponding area were removed by a reactive ion etching (RIE) process with the photoresist AZ5214 as the shadow mask. After the pattern was properly defined, two large rectangular windows (9 mm× 8.5 mm) on the sides and a narrow rectangular window (34 μ m× 23 mm) in the middle of the device were etched utilizing RIE process (Technics 85 Reactive Ion Etcher, 190 mTorr, 150W, 6 minutes) to expose the tails and tips of the sensing electrodes respectively (Fig. 2g).

Moreover, to develop the obstacles, as trapping zones, a layer of negative photoresist SU-8 2050 was spin-coated at 3000 rpm for 30 seconds to obtain a 50 μ m film (Fig. 2h). Prior to SU-8 coating, a thin layer of OmniCoat was spin-coated at 3000 rpm for 30 seconds to allow easy stripping of SU-8 and improve the adhesion. The SU-8 layer was exposed under 160 mJ/cm² ultraviolet light with a mask and developed with SU-8 developer to create triangular obstacles with 10 μ m width separation (Fig. 2i). RIE was then performed to remove the residual OmniCoat (Fig. 2j). Polydimethylsiloxane (PDMS) chamber was created by pouring the mixture of silicone elastomer base and curing agent (volume ratio 10 to 1) on a glass slide and heating up to 70°C for 4 hours. After the PDMS was fully crosslinked, it was peeled off from the glass slide and cut into rectangular pieces with 2 cm in width and 4 cm in length. Six holes with diameter of 3.5 mm were punched as the inlets and outlets. At the final stage, the PDMS chamber was adhered on the device to cap the SU-8 obstacles and create the opening with the dimension of 10 μ m ×50 μ m. A heat seal connector was used to connect the tail of the electrodes on the microchip to a home-designed PCB board. The PCB board was then connected to the power supply and the digital impedance analyzer to apply voltage and conduct the impedance measurement.

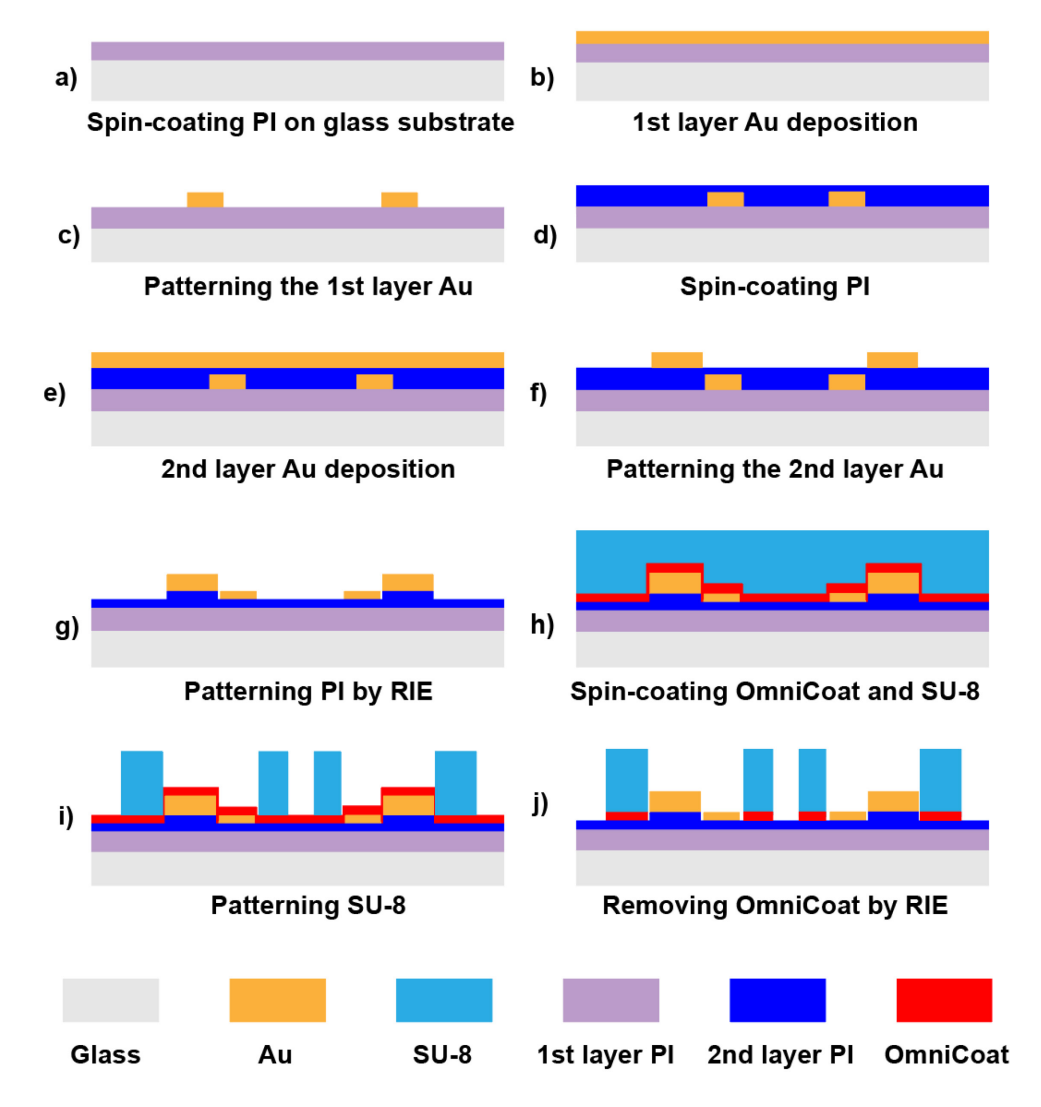


Figure 2. Step by step fabrication procedure of proposed LOC device.

2.4. Particle trapping and Impedance Measurement

 $25~\mu L$ of electrolyte solution containing different particles including 1.8×10^8 /mL and 2.3×10^{12} /mL COOH-PS beads, 1.9×10^{11} /mL liposomes, and 6.1×10^9 /mL exosomes were injected in to different device chambers. A 5V/mm DC bias was applied across the trapping electrodes using a Keithley 2220G-30-1 voltage generator for 5 minutes. The microscopic images were recorded using an inverted microscope, Olympus IX71, equipped with a high-resolution camera, Andor NeoZyla 5.5.

Impedance measurement was conducted utilizing the digital impedance analyzer (HF2LI, Zurich Instrument) as an AC field with a peak amplitude of 100 mV swept from 1 kHz to 10 MHz to record the magnitude and phase components at each frequency. Afterwards, the data was processed with a custom script written in MATLAB (MathWorks Inc., Natick, MA, USA) for statistical analysis. The impedance signals were recorded at a sampling rate of 225 sample/sec. Each measurement was repeated at least 3 times. Furthermore, to rule out the effect of the particles concentration and to demonstrate the difference between the particles dielectric properties, the impedance was normalized based on the 'opacity' concept which was reported by Gawad et. al. (Equ. 1)[11,19,20]

$$O_f = \frac{Z(f)}{Z(0.5 MHz)} \tag{1}$$

where Z(f) and $Z(0.5\,MHz)$ are the impedance magnitude measured at frequencies higher than 0.5 MHz and at 0.5 MHz respectively. This has been widely applied in cell cytometry to normalize the impedance with respect to the cell size and position since the impedance at 0.5 MHz typically reflects the particle size information. [5,9,20,21]

149 Statistical analysis was performed using the student's t-test and two-way analysis of variance. 150 Difference with p-values less than 0.05 were considered significant.

2.5. Finite element analysis

151

152

153

154

155

156

157

158

159

162

163

164

165

166

167

168

169

170

171

172

173

174

175

176

178

179

180

181

182

183

184

185

186

187

188 189

190

191

192

193

194

Finite-element software, COMSOL Multiphysics 5.2a (COMSOL Inc, Burlington, MA, USA), was utilized to determine the distribution of the electric field gradient as 5V/mm DC was applied across the gap which was created by SU-8 obstacles. The height of the SU-8 obstacles was 50 μ m and the gap distance between a pair of triangular SU-8 obstacles was 10 µm. The conductivity and relative permittivity of the suspending solution in the model was set as 0.3 S/m and 80 to mimic the conductivity of 10 mM KCl solution. The temperature and pressure were assumed to be 298 K and zero Pa, respectively.

The migration mobility of ionic species (*u*) was computed using the Nernst-Einstein relation (2):

160
$$u = \frac{D_i}{RT}$$
 (2)
161 in which, D_i is the diffusion coefficient, R is the molar gas constant and T is the absolute temperature.

For 10 mM KCl, the value of D_i was set as 2×10^{-9} m²s⁻¹.

Boundary conditions corresponding to the solution obtained from the Poisson-Boltzmann equation for electric potential were applied. The boundary conditions established that the electric potential was not diverged and the gradient of this potential on the SU-8 surface varied with the change in surface charge density.[22]

2.6. Theoretical modeling and equivalent circuit

A simplified equivalent circuit model (Fig 3.) was used to demonstrate the physical principle of the impedance measurement system. [23-25] In this model, the channel impedance Zch is in series with an electrical double layer capacitance Cdl and is in parallel with a stray capacitance Cstray. [23-25] In addition, a lead inductance (Lid), which is introduced by the impedance analyzer connecting cables, is included in the equivalent circuit. The values of Cdl, Cstray and Lld were obtained via measurements on electrolyte solutions with well-known electrical properties, followed by fitting into the combination of constant phase element and Cole-Cole model.[26,27] Fitting parameters that were used throughout this theoretical modeling were C_{dl} = 10 pF, C_{stray} = 2.2 pF, and L_{ld} = 6 μ H, respectively.

Channel impedance Z_{ch} was calculated based on Maxwell's mixture theory (Equ. 3).[13,28]

$$\tilde{Z}_{ch} = \frac{1}{j\omega\tilde{\varepsilon}_{mix}G_f} \tag{3}$$

where $\tilde{\epsilon}_{mix}$ is the equivalent complex permittivity of the mixture of particles and the medium, ω is the angular frequency, and G_f is the geometrical constant of the system.

The equivalent complex permittivity of mixture of homogeneous spherical particles in suspension can be calculated as:

$$\tilde{\varepsilon}_{mix} = \tilde{\varepsilon}_m \frac{1 + 2\phi \tilde{f}_{CM}}{1 - \phi \tilde{f}_{CM}} \tag{4}$$

where ϕ is the volume fraction (the volume ratio between the particle and the suspending system), which is estimated as 0.1 for COOH-PS based on the estimated size of entrapped particles cluster under the microscopy; \tilde{f}_{CM} is the complex Clausius-Mossotti factor, which is defined as:

$$\tilde{f}_{CM} = \frac{\tilde{\varepsilon}_p - \tilde{\varepsilon}_m}{\tilde{\varepsilon}_p + 2\tilde{\varepsilon}_m} \tag{5}$$

where $\tilde{\varepsilon}_m$ and $\tilde{\varepsilon}_p$ are the complex permittivity of the suspending medium and particle respectively; and $\tilde{\varepsilon} = \varepsilon - \frac{j\sigma}{\omega}$ where $j^2 = -1$, ε and σ are permittivity and conductivity. The relative permittivity and conductivity of the 100 nm polystyrene beads are set as 2.55 and 7.2 mS/m, respectively. [17,29-32]

The geometrical constant G_f in Equ.3 can be presented as $G_f = \kappa w$,[13] where w is the width of the electrode and κ is the correction factor describing the fringing field. The value of κ was derived analytically using the conforming mapping method. [13,33,34] Utilizing this method, κ and geometric constant G_f were calculated as 0.73 and 7.3 μ m, respectively (the details of the derivation is provided in supplementary information (Fig. S1)).

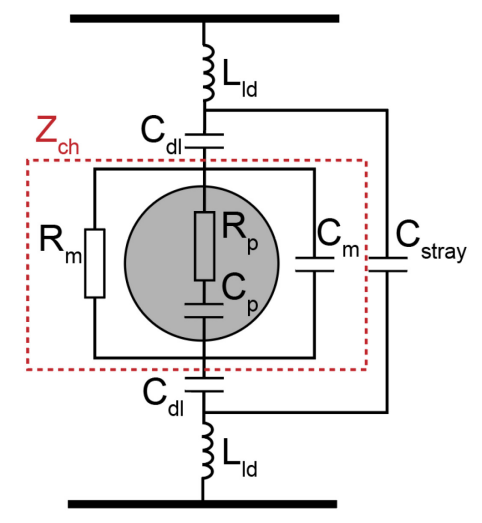


Figure 3. An equivalent circuit model for the impedance measurement system.

3. Results and Discussion

3.1. Particles entrapment

In our previous work, we have demonstrated that COOH-PS beads, liposomes and exosomes with sub-micron diameters could be rapidly trapped at the tip of a glass micropipette due to the balance of DEP, EP and EOF forces.[17,18] Others have also reported that the micro-pores constructed by SU-8 or PDMS triangles are effective geometrical designs to isolate particles and cells utilizing electrokinetics.[35,36] Here, to integrate the trapping mechanism with the sensing module on a single chip (Fig. 4a), we developed a SU-8 constructed micro-pores with 10 μ m width and 50 μ m height to trap particles utilizing DEP. Furthermore, a pair of co-planar electrodes (12 μ m × 10 μ m with 10 μ m gap distance) were fabricated to measure the impedance of the trapped particles (Fig. 4b). A finite element simulation was carried out to study the distribution of the electric field (E-field) gradient under DC bias (Fig. 4c). The results illustrated that the highest E-field gradient was localized at the narrowest part of the opening, which was consistent with our previous study.[36]

A series of experiments were conducted with fluorescently-tagged COOH-PS beads, fluorescently-tagged liposomes, and exosomes suspended in 10 mM KCl (pH 7.0). 25 μ L solution containing various particles were injected separately in to different chambers of the device and 5V/mm DC bias was applied across the opening for 5 minutes. Fig. 4d and S2 show that the particles were trapped at the narrowest region of the opening as expected.

217

218

219

220

221

222

223

224

225

226

227

228

229

230

231

232

233

234

235

236

237

238

239

240

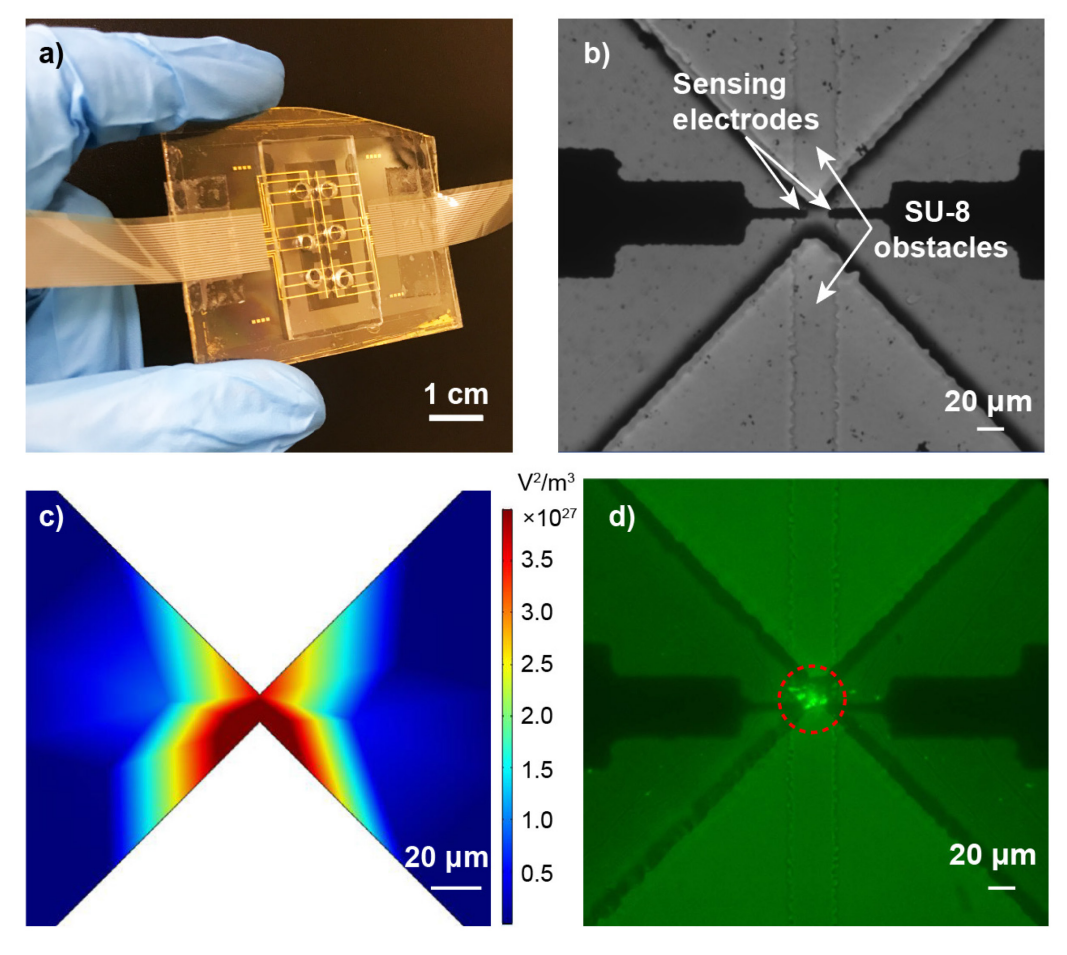


Figure 4. a) The LOC device. **b)** The bright-field microscopic image of the device. **c)** The finite element analysis of the distributioan of the electric field gradient across the opening created by SU-8; the suspending medium was 10 mM KCl and the applied voltage was 5V/mm. **d)** The fluorescence microscopic images showing the entrapment of 100 nm fluourencently tagged COOH-PS beads with a 5V/mm bias applied across the opening for 5 minutes; the initial particle concentration was 2.3×10¹² /mL and the suspending solution was 10 mM KCl.

3.2. Impedance measurement of solution with various ionic strengths

To study the capability of the device to differentiate between solutions with different ionic strengths, and understand the physical principle of the impedance measurement, an equivalent circuit model was constructed and the theoretical and experimental results were compared. Fig. 5a demonstrates both the theoretical and experimental results of the impedance when solutions with different conductivities were tested. The theoretical results were closely matched with the experimental measurements, which implies that the established equivalent circuit model was reliable for predicting the impedance of the system. In addition, the results were in line with the previously reported observations [37-40] and suggested that as the frequency increased, the absolute value of impedance decreased for all solutions. This is due to the fact that the reactive part of the impedance was predominately capacitive and thus, the co-planar impedance sensor acted as a capacitor, storing electrochemical energy.[38] Statistical data obtained from the experimental measurements show in Table S1 indicates that the impedance of the solutions were significantly different from each other (p <0.05) at a wide frequency spectrum, and thus, the device is capable of differentiating solutions with different ionic strengths. However, the results also indicate that the impedance of the solutions with 1.4 S/m and 5.9 S/m conductivities at frequency ≥ 10 MHz were not significantly different from each other. This could be justified since the stray capacitance is dominated at frequency ≥ 10 MHz which resulted in the reduction of the difference in their impedance .[41] In addition, to further investigate the capability of the circuit model to predict the impedance of the particles, theoretical results and

experimental measurements were compared utilizing the well-defined 100 nm COOH-PS beads suspended in 10 mM KCl. Figure. 5b demonstrates that the theoretical results were closely matched with the experimental measurements, which proves that the established equivalent circuit model is reliable for predicting the impedance of the system with added beads.

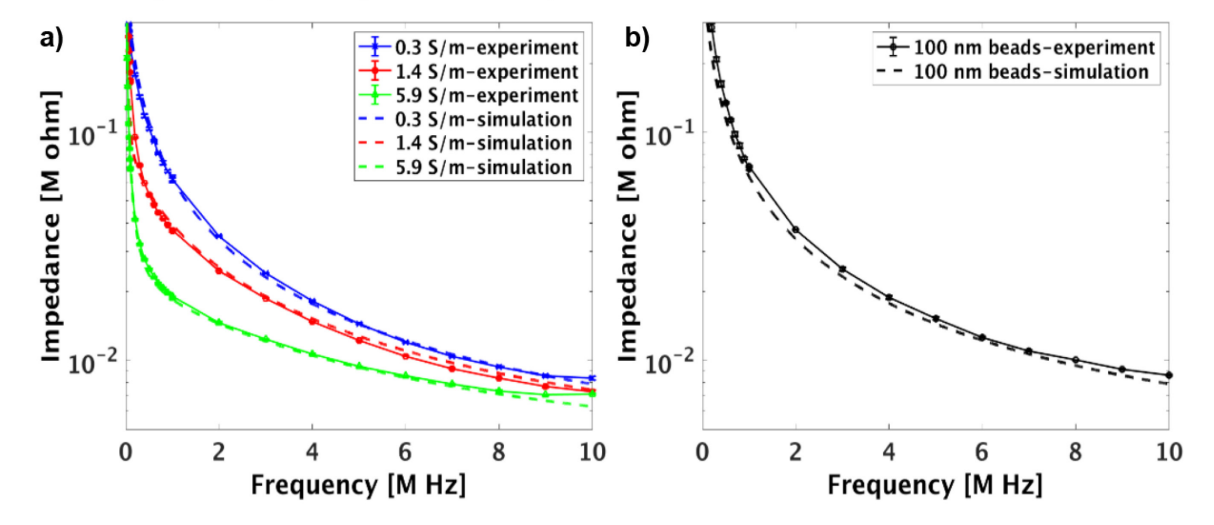


Figure 5. a) The theoretical modeling and experimental results showing the impedance of soluitons with different conductivities as a function of frequency. **b)** The theoretical modeling and experimental results showing the impedance of COOH-PS beads suspended in 10 mM KCl. The error bars represented the standard deviation and each experiment was repeated for at least three times.

3.3. Impedance measurements of sub-micron particles in solution

To investigate the impedance response of different sub-micron particles, COOH-PS beads, liposomes, and exosomes, suspended in 10 mM KCl were injected in to different chambers of the device. The particles were trapped at the triangular trapping zones by applying DC bias, and their impedance were recorded under AC field. The impedance of the entrapped liposomes and COOH-PS beads were increased when compared to the solution containing no particles (Fig. 6a). This result could be justified since the lipid bilayer in liposome and the bulk polystyrene materials in COOH-PS beads have lower conductivities when compared to the surrounding medium, and thus, resulting in the enhancement of the channel resistance.[42,43] However, as exosomes were incorporated in to the system, a lower impedance was measured which suggested that exosomes were more conductive than the suspending medium, which is because proteins with a relatively high conductivity are embedded on exosomes' membrane.[44,45]

To further study the impedance response of the particles with different concentration, COOH-PS beads with different initial concentration (1.8×10^8 /mL and 2.3×10^{12} /mL) were injected into different chambers of the LOC device and trapped by applying 5 V/mm DC field for 5 minutes. The results in Fig. 6b and Table S2 show that as the initial concentration of COOH-PS beads was increased, more beads were trapped at the triangular trapping zone (the microscopic images) and the impedance of the system significantly increased due to the enhancement of the channel resistance and the reduction of channel capacitance.[42]

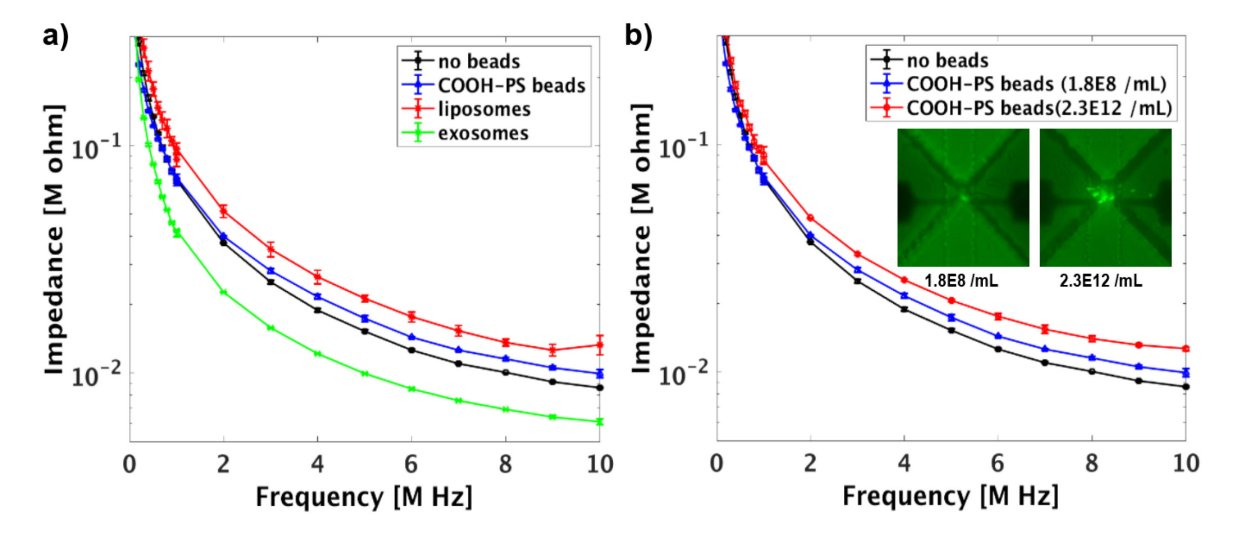


Figure 6. a) The impedance of different particles suspended in electrolytic (10 mM KCl) solution as a function of frequency. **b)** The impedance of the COOH-PS beads with different initial concentrations suspended in 10 mM KCl solution. The error bars represented the standard deviation and each experiment was repeated for at least three times.

To rule out the effect of the particles' concentration on their impedance and only show the effect of their dielectric properties by impedance measurements, the results were normalized based on the opacity concept.[3,11,19] The impedance of the COOH-PS beads with different initial concentration $(1.8\times10^8 \, / \text{mL})$ and $2.3\times10^{12} \, / \text{mL})$ were normalized based on opacity magnitude and plotted in Fig. 7a and summarized in Table S3. The results demonstrate that there were no significant differences (p >0.05) between the opacities of COOH-PS beads with different initial concentrations.

To further investigate the capability of the system to differentiate between particles with different dielectric properties, the opacity magnitude of three types of particles with different compositions were analyzed and plotted in Fig. 7b. A detailed representation of the data with statistical analysis are shown in Table S4. The results show that COOH-PS beads and exosomes were differentiated at frequency range ≥ 1 MHz, and COOH-PS beads and liposomes were differentiated at the frequency range ≥ 2 MHz. This results indicate that the dielectric properties of the COOH-PS beads is vastly different from the nanovesicles due to the difference of composition and surface charge (Table S5).[9,20] In addition, liposomes and exosomes could be differentiated at the frequency range ≥ 6 MHz, which most likely reflects on their membrane capacitance differences due to the presence of proteins on exosomes' membrane.[9,20,44]

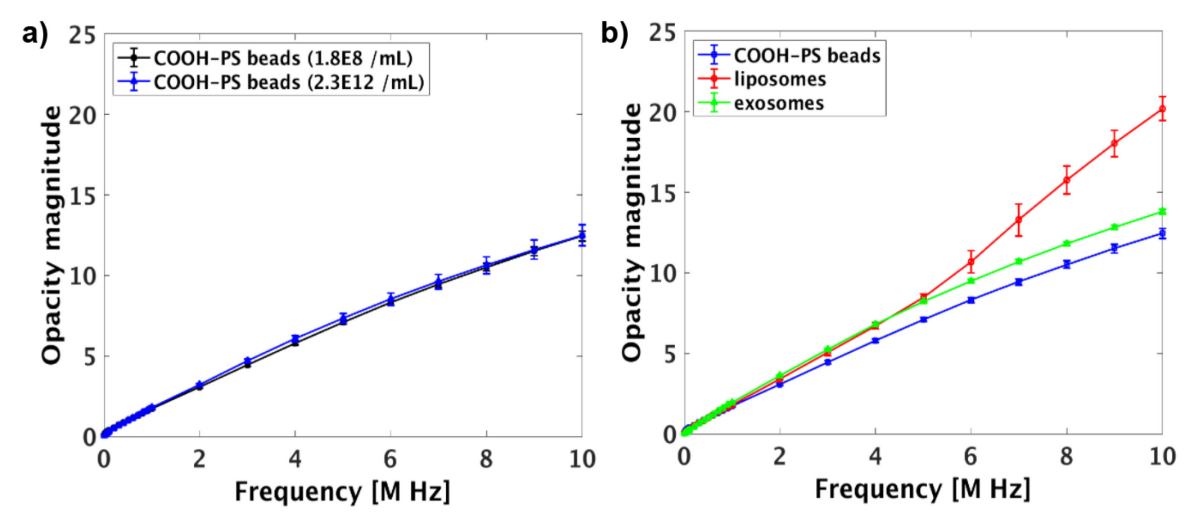


Figure 7. a) The opacity magnitude of 100 nm COOH-PS beads with different entrapped quantities.

b) Opacity magnitude of different particles suspended in 10 mM KCl. The error bars represented the standard deviation and each experiment was repeated for at least three times.

4. Conclusions

292

293

294

295

296

297

298

299

300

301

302

303

304

305

306

307

308

309

In this study, we have demonstrated a microchip device which is capable of entrapment of nanovesicles utilizing an insulator-based dielectrophoretic (iDEP) module and an integrated impedance measurement system to characterize the nanovesicles bases on their dielectric properties. The device is comprised of SU-8 obstacles to create micron-size openings to create a non-uniform electric field in order to entrap particles as a result of the balance of three electrokinetic forces under DC bias. The entrapped particles could be further analyzed based on their impedance by an integrated co-planar sensor under AC field and a wide frequency spectrum. The impedance of solution with different ionic strengths and the well-defined COOH-PS beads were measured to validate our empirical results and the results were matched with the theoretical equivalent circuit model. Also, the results obtained by analysis of nanoparticles (COOH-PS) and nanovesicles (liposomes and exosomes) of similar size, demonstrated that the device is capable of discriminating between different particles with different compositions and hence, different dielectric properties at frequency range of ~2 to 10 MHz. As a result, the proposed device could potentially be applied for characterization and detection of pathogenic nanovesicles based on their unique dielectric properties, and thus, further evolved as a powerful tool for early disease diagnosis and prognosis.

- 310 Supplementary Materials: The following are available online at www.mdpi.com/xxx/s1, Figure S1: Diagrams 311 showing the conformal transformation from physical plane (x,z) to model plane (u,v). Figure S2: a) The 312 microscopic images of entrapped fluorescently-tagged liposomes. b) The microscopic images of entrapped 313 hTERT Mesenchymal Stem Cell Exosomes. A 5V/mm bias was applied across the channel for 5 minutes and the 314 suspending solution was 10 mM KCl. Table S1: The statistical data for the impedance measurement of different 315 electrolyte solutions. p-values were obtained from two-tails unpaired student t-test. The highlighted data are 316 significantly different. Table S2: The statistical data for the impedance measurement of different particles 317 suspended in 10 mM KCl. p-values were obtained from two-tails unpaired student t-test. The highlighted data 318 are significantly different. Table S3: The statistical data for the opacity magnitude of COOH-PS beads with 319 different concentration suspended in 10 mM KCl. p-values were obtained from two-tails unpaired student t-test. 320 Table S4: The statistical data for the opacity magnitude of different particles suspended in 10 mM KCl. p-values 321 were obtained from two-tails unpaired student t-test. The highlighted data are significantly different. Table S5: 322 Zeta potential of COOH-PS beads, liposomes, and exosomes suspended in 10 mM KCl.
- Author Contributions: L.S. carried out the experiments, analyzed tata, wrote/edited the main body of the manuscript, and provided intellectual input. L.E. designed the study, gave instructions and suggestions on the experiments and manuscript writing, and provided intellectual input. All authors read and gave final approval of the manuscript.
- 327 **Funding:** This research was funded by NSF EAGER ECCS (2020112).
- 328 Acknowledgments: The authors thank Yuqian Zhang for helping analyze data and Shreyak Shah for doing finite
- 329 element analysis. We also thank Jeffrey Simkins and Ronald Flenniken for their kindly assistance on device
- 330 fabrication.
- Conflicts of Interest: The authors declare no conflict of interest.

332 References

- 333 1. Sohn, L.; Saleh, O.; Facer, G.; Beavis, A.; Allan, R.; Notterman, D.A. Capacitance cytometry: Measuring biological cells one by one. *Proceedings of the National Academy of Sciences* **2000**, 97, 10687-10690.
- MacCuspie, R.I.; Nuraje, N.; Lee, S.-Y.; Runge, A.; Matsui, H. Comparison of electrical properties of viruses studied by AC capacitance scanning probe microscopy. *Journal of the American Chemical Society* 2008, 130, 887-891.
- 338 3. Holmes, D.; Pettigrew, D.; Reccius, C.H.; Gwyer, J.D.; van Berkel, C.; Holloway, J.; Davies, D.E.; Morgan, H. Leukocyte analysis and differentiation using high speed microfluidic single cell impedance cytometry. *Lab on a Chip* **2009**, *9*, 2881-2889.

- 4. Chen, N.-C.; Chen, C.-H.; Chen, M.-K.; Jang, L.-S.; Wang, M.-H. Single-cell trapping and impedance measurement utilizing dielectrophoresis in a parallel-plate microfluidic device. *Sensors and Actuators B: Chemical* **2014**, 190, 570-577.
- Haandbæk, N.; Bürgel, S.C.; Heer, F.; Hierlemann, A. Characterization of subcellular morphology of single yeast cells using high frequency microfluidic impedance cytometer. *Lab on a Chip* **2014**, *14*, 369-377.
- Höber, R. Eine Methode, die elektrische Leitfähigkeit im Innern von Zellen zu messen. Pflüger's Archiv für die gesamte Physiologie des Menschen und der Tiere 1910, 133, 237-253.
- 7. Fricke, H. The electric capacity of suspensions with special reference to blood. *The Journal of general physiology* **1925**, *9*, 137-152.
- 350 8. Curtis, H.J.; Cole, K.S. Transverse electric impedance of Nitella. *The Journal of general physiology* **1937**, 21, 189-201.
- McGrath, J.; Honrado, C.; Moore, J.; Adair, S.; Varhue, W.; Salahi, A.; Farmehini, V.; Goudreau, B.; Nagdas,
 S.; Blais, E. Electrophysiology-based Stratification of Pancreatic Tumorigenicity by Label-free Single-Cell
 Impedance Cytometry. Analytica Chimica Acta 2019.
- 10. Cho, Y.H.; Yamamoto, T.; Sakai, Y.; Fujii, T.; Kim, B. Development of microfluidic device for electrical/physical characterization of single cell. *Journal of Microelectromechanical Systems* **2006**, 15, 287-295.
- 357 11. Gawad, S.; Schild, L.; Renaud, P. Micromachined impedance spectroscopy flow cytometer for cell analysis and particle sizing. *Lab on a Chip* **2001**, *1*, 76-82.
- Holmes, D.; Morgan, H. Single cell impedance cytometry for identification and counting of CD4 T-cells in human blood using impedance labels. *Analytical chemistry* **2010**, *82*, 1455-1461.
- 361 13. Sun, T.; Bernabini, C.; Morgan, H. Single-colloidal particle impedance spectroscopy: Complete equivalent circuit analysis of polyelectrolyte microcapsules. *Langmuir* **2009**, *26*, 3821-3828.
- 363 14. Ayliffe, H.E.; Frazier, A.B.; Rabbitt, R. Electric impedance spectroscopy using microchannels with integrated metal electrodes. *Journal of Microelectromechanical systems* **1999**, *8*, 50-57.
- 365 15. Iliescu, C.; Poenar, D.P.; Carp, M.; Loe, F.C. A microfluidic device for impedance spectroscopy analysis of biological samples. *Sensors and Actuators B: Chemical* **2007**, *123*, 168-176.
- 367 16. Zong, X.; Zhu, R.; Guo, X. Nanostructured gold microelectrodes for SERS and EIS measurements by incorporating ZnO nanorod growth with electroplating. *Scientific reports* **2015**, *5*, 16454.
- 369 17. Shi, L.; Rana, A.; Esfandiari, L. A low voltage nanopipette dielectrophoretic device for rapid entrapment of nanoparticles and exosomes extracted from plasma of healthy donors. *Scientific reports* **2018**, *8*, 6751.
- 371 18. Shi, L.; Kuhnell, D.; Borra, V.J.; Langevin, S.M.; Nakamura, T.; Esfandiari, L. Rapid and label-free isolation of small extracellular vesicles from biofluids utilizing a novel insulator based dielectrophoretic device. *Lab on a Chip* **2019**.
- 374 19. Gawad, S.; Cheung, K.; Seger, U.; Bertsch, A.; Renaud, P. Dielectric spectroscopy in a micromachined flow cytometer: theoretical and practical considerations. *Lab on a Chip* **2004**, *4*, 241-251.
- Chen, J.; Xue, C.; Zhao, Y.; Chen, D.; Wu, M.-H.; Wang, J. Microfluidic impedance flow cytometry enabling
 high-throughput single-cell electrical property characterization. *International journal of molecular sciences* 20. Chen, J.; Xue, C.; Zhao, Y.; Chen, D.; Wu, M.-H.; Wang, J. Microfluidic impedance flow cytometry enabling
 high-throughput single-cell electrical property characterization. *International journal of molecular sciences* 2015, 16, 9804-9830.
- Norlin, A.; Pan, J.; Leygraf, C. Investigation of interfacial capacitance of Pt, Ti and TiN coated electrodes by electrochemical impedance spectroscopy. *Biomolecular Engineering* **2002**, 19, 67-71, doi:https://doi.org/10.1016/S1389-0344(02)00013-8.
- 22. Laohakunakorn, N.; Thacker, V.V.; Muthukumar, M.; Keyser, U.F. Electroosmotic flow reversal outside glass nanopores. *Nano letters* **2015**, *15*, 695-702.
- 23. Zheng, S.; Liu, M.; Tai, Y.-C. Micro coulter counters with platinum black electroplated electrodes for human blood cell sensing. *Biomedical microdevices* **2008**, *10*, 221-231.
- 386 24. Guo, X.; Zhu, R.; Zong, X. A microchip integrating cell array positioning with in situ single-cell impedance measurement. *Analyst* **2015**, *140*, 6571-6578.
- Robinson, D.A. The electrical properties of metal microelectrodes. *Proceedings of the IEEE* **1968**, *56*, 1065-1071.
- 390 26. Yoon, G. Dielectric properties of glucose in bulk aqueous solutions: Influence of electrode polarization and modeling. *Biosensors and Bioelectronics* **2011**, *26*, 2347-2353.
- 392 27. Schwan, H. Electrode polarization impedance and measurements in biological materials. *Annals of the New York Academy of Sciences* **1968**, *148*, 191-209.

- 394 28. Maxwell, J.C. Preface to the First Edition, A Treatise on Electricity and Magnetism, Vol. 1. Dover Publications, New York: 1954.
- 396 29. Zheng, L.; Brody, J.P.; Burke, P.J. Electronic manipulation of DNA, proteins, and nanoparticles for potential circuit assembly. *Biosensors and Bioelectronics* **2004**, *20*, 606-619.
- 398 30. Krishnan, R.; Sullivan, B.D.; Mifflin, R.L.; Esener, S.C.; Heller, M.J. Alternating current electrokinetic separation and detection of DNA nanoparticles in high-conductance solutions. *Electrophoresis* **2008**, 29, 1765-1774.
- Weng, P.-Y.; Chen, I.-A.; Yeh, C.-K.; Chen, P.-Y.; Juang, J.-Y. Size-dependent dielectrophoretic crossover frequency of spherical particles. *Biomicrofluidics* **2016**, *10*, 011909.
- 403 32. Cui, L.; Holmes, D.; Morgan, H. The dielectrophoretic levitation and separation of latex beads in microchips. *Electrophoresis* **2001**, 22, 3893-3901.
- 405 33. Hong, J.; Yoon, D.S.; Kim, S.K.; Kim, T.S.; Kim, S.; Pak, E.Y.; No, K. AC frequency characteristics of coplanar impedance sensors as design parameters. *Lab on a Chip* **2005**, *5*, 270-279.
- 407 34. Sun, T.; Green, N.G.; Gawad, S.; Morgan, H. Analytical electric field and sensitivity analysis for two microfluidic impedance cytometer designs. *IET nanobiotechnology* **2007**, *1*, 69-79.
- 409 35. Jen, C.-P.; Chen, T.-W. Selective trapping of live and dead mammalian cells using insulator-based dielectrophoresis within open-top microstructures. *Biomedical microdevices* **2009**, *11*, 597.
- 411 36. Chiou, C.-H.; Pan, J.-C.; Chien, L.-J.; Lin, Y.-Y.; Lin Jr, -.L. Characterization of microparticle separation utilizing electrokinesis within an electrodeless dielectrophoresis chip. *Sensors* **2013**, *13*, 2763-2776.
- 413 37. Li, Q.; Yuan, Y. Application of vertical electrodes in microfluidic channels for impedance analysis.

 414 *Micromachines* **2016**, 7, 96.
- 415 38. Tsai, S.L.; Wang, M.H.; Chen, M.K.; Jang, L.S. Analytical and numerical modeling methods for electrochemical impedance analysis of single cells on coplanar electrodes. *Electroanalysis* **2014**, *26*, 389-398.
- 417 39. Iliescu, C.; Poenar, D.P.; Selvan, S.T. Frequency dependence on the accuracy of electrical impedance spectroscopy measurements in microfluidic devices. *Journal of Micromechanics and Microengineering* **2009**, 419 20,022001.
- 420 40. Jang, L.-S.; Wang, M.-H. Microfluidic device for cell capture and impedance measurement. *Biomedical microdevices* **2007**, *9*, 737-743.
- 422 41. Gómez, R.; Bashir, R.; Bhunia, A.K. Microscale electronic detection of bacterial metabolism. *Sensors and Actuators B: Chemical* **2002**, *86*, 198-208.
- 424 42. Haandbæk, N.; Bürgel, S.C.; Heer, F.; Hierlemann, A. Resonance-enhanced microfluidic impedance cytometer for detection of single bacteria. *Lab on a Chip* **2014**, *14*, 3313-3324.
- 426 43. Chan, K.L.; Gascoyne, P.R.; Becker, F.F.; Pethig, R. Electrorotation of liposomes: verification of dielectric multi-shell model for cells. *Biochimica et Biophysica Acta (BBA)-Lipids and Lipid Metabolism* **1997**, 1349, 182-196.
- 429 44. Tamkovich, S.; Tutanov, O.; Laktionov, P. Exosomes: Generation, structure, transport, biological activity, and diagnostic application. *Biochemistry (Moscow) Supplement Series A: Membrane and Cell Biology* **2016**, *10*, 163-173.
- 432 45. Clarke, R.W.; Piper, J.D.; Ying, L.; Klenerman, D. Surface conductivity of biological macromolecules measured by nanopipette dielectrophoresis. *Physical review letters* **2007**, *98*, 198102.
- 434 **Publisher's Note:** MDPI stays neutral with regard to jurisdictional claims in published maps and institutional affiliations.



© 2020 by the authors. Submitted for possible open access publication under the terms and conditions of the Creative Commons Attribution (CC BY) license (http://creativecommons.org/licenses/by/4.0/).